Temperature-dependent VNIR spectroscopy of hydrated Mg-sulfates

S. De Angelis[1], C. Carli[1], F. Tosi[1], P. Beck[2], B. Schmitt[2], G. Piccioni[1], M.C. De Sanctis[1], F. Capaccioni[1], T. Di Iorio[3], Sylvain Philippe[2]

[1]Istituto di Astrofisica e Planetologia Spaziali, INAF-IAPS, Via del Fosso del Cavaliere 100, I-00133 Roma, Italy

[2]Institut de Planétologie et d'Astrophysique de Grenoble (IPAG), 414 Rue de la Piscine, F-38400 St-Martin d'Hères (France), France

[3]ENEA Centro Ricerche Casaccia (ENEA SSPT-PROTER-OAC), Via Anguillarese 301, I-00123 Roma, Italy

Abstract

We investigate two poly-hydrated magnesium sulfates, hexahydrite ($MgSO_4 \cdot 6H_2O$) and epsomite ($MgSO_4 \cdot 7H_2O$), in the visible and infrared (VNIR) spectral range 0.5÷4.0 μm, as particulate for three different grain size ranges: 20-50 μm, 75-100 μm and 125-150 μm. All samples were measured in the 93 K to 298 K temperature range. The spectra of these hydrated salts are characterized by strong OH absorption bands in the 1.0-1.5 μm region, and by H_2O absorption bands near 2 and 3 μm. Other weak features show up at low temperatures near 1.75 μm (in both hexahydrite and epsomite) and 2.2 μm (only in hexahydrite). The spectral behavior of the absorption bands of these two minerals has been analyzed as a function of both grain size and temperature, deriving trends related to specific spectral parameters such as band center, band depth, band area, and band width. Hydrated minerals, in particular mono- and poly-hydrated sulfates, are present in planetary objects such as Mars and the icy Galilean satellites. Safe detection of these minerals shall rely on detailed laboratory investigation of these materials in different environmental conditions. Hence an accurate spectral analysis of such minerals as a function of temperature is key to better understand and constrain future observations.

Keywords. Mars. Europe. Sulfates. VNIR spectroscopy. JUICE.

1. Introduction

Sulfate minerals in different states of hydration are present in the Solar System. Combined in situ measurements, remote-sensing observations and laboratory investigations carried out in recent years have allowed to detect hydrated sulfates on Mars (Brueckner 2004; Gendrin et al., 2005;

Chevrier and Mathè, 2006; Murchie et al., 2009; Ehlmann et al., 2014) and on icy satellites like Europa and Ganymede (McCord et al., 1999; McCord et al., 2001; Dalton et al., 2005). Nathues et al. (2015) suggested the presence of hydrated sulfates on the dwarf planet Ceres based on Dawn observations.

Sulfates on Earth can originate from different geologic processes, such as: (i) precipitation due to water evaporation in lakes or sabkhas environments, (ii) interaction rocks-acidic groundwater in hydrothermal environments, and (iii) aqueous alteration of volcanic products (Warren, 2006, 2010). On the Earth, magnesium sulfate has three stable hydration states: kieserite ($MgSO_4 \cdot H_2O$), hexahydrite ($MgSO_4 \cdot 6H_2O$) and epsomite ($MgSO_4 \cdot 7H_2O$). It has been shown (Vaniman et al., 2004) that kieserite is easily hydrated at high relative humidity conditions (>55% RH) and converted in hexahydrite and epsomite, although the reverse transformation upon desiccation is unlikely. Moreover hexahydrite and epsomite tend to transform to an amorphous phase when subject to rapid dehydration and pressure reduction (Vaniman et al., 2004; Wang et al., 2006; Cloutis et al., 2007), and tend to dehydrate when exposed to UV radiation (Cloutis et al., 2007).

Mars. According to Feldman et al. (2004), who studied the distribution of subsurface epithermal neutrons, various hydrated states of magnesium salts could be present at equatorial latitudes on Mars. Brueckner (2004) described layered outcrops in Meridiani Crater containing sulfate as cementation agent. Based on OMEGA (Mars Express; Bibring et al., 2004) observations, Gendrin et al. (2005) proposed magnesium mono-hydrated (kieserite) and poly-hydrated (epsomite) sulfates to occur, together with calcium sulfates, in outcrops in several Martian layered terrains, located in Valles Marineris, Margaritifer Sinus and Terra Meridiani (Chevrier and Mathè, 2006). However, the same OMEGA data could be well fitted with iron poly-hydrated sulfates. Generally kieserite and poly-hydrated sulfates occur as light deposits in these layered terrains. Kieserite and poly-hydrated sulfate phases have also been suggested by the observations of CRISM (Mars Reconnaissance Orbiter; Murchie et al., 2007) in Meridiani Planum and Valles Marineris layered deposits (Murchie et al., 2009; Weitz et al., 2015) and in paleolakes (Wray et al., 2009). However it is still poorly understood if hydrated phases are stable under all Martian conditions and during daytime and seasonal cycles (Roach et al., 2009). Mars Science Laboratory instruments onboard Curiosity rover have detected mainly hydrated calcium-sulfates at Yellowknife Bay (Rice et al., 2013; Nachon et al., 2013).

Icy Galilean satellites. The presence of hydrated salts of magnesium on the surface of Europa has been suggested on the basis of Galileo/NIMS spectra (McCord et al., 1998; McCord et al., 1999; McCord et al., 2010). McCord et al. (1998) argued that the presence of hexahydrite and epsomite on Europa (as well as of other sulfates) could be explained by hydrothermal activity related to the subsurface ocean and consequent material upwelling. NIMS spectra of Europa's reddish plains are thought to resemble those of hydrated magnesium sulfates with a high number of water molecules (Dalton et al., 2005), although it has been pointed out that Europa's non-icy terrains are likely composed of mixtures of different types of sulfates (McCord et al., 1999). Best fits for non-icy terrains on Europa are indeed provided by mixtures of hexahydrite, bloedite ($Na_2Mg(SO_4)_2 \cdot 4H_2O$), mirabilite ($Na_2SO_4 \cdot 10H_2O$), and sulfuric acid hydrate ($H_2SO_4 \cdot nH_2O$) (Dalton, 2007). Carlson

et al. (2009) alternatively suggested that the surface of Europa is mainly constituted by poly-hydrated sulfuric acids, produced after irradiation of SO_2 in water ice.

Meteorites. Hydrated Mg-sulfates (epsomite) have also been identified in the matrices of carbonaceous chondrites (Burgess et al., 1991) after stepped combustion experiments. Other authors report various types of sulfates also in veins and grains in carbonaceous chondrites (Fredriksson and Kerridge, 1988; Brearley and Jones, 1998). Hutchison (2006) reports the presence of epsomite particularly in veins and matrices of CI carbonaceous chondrites, although some authors (Gounelle and Zolensky, 2001) assess that some of the sulfates in CI1 chondrites could have formed by terrestrial alteration.

Laboratory investigations. Laboratory studies have shown that the main diagnostic absorption features in VNIR spectra of hydrated sulfates do not undergo dramatic changes in position when exposed to simulated Martian conditions (Cloutis et al., 2007), while major changes in bands' shapes and parameters occur at cryogenic temperatures (Dalton et al., 2005). Band parameters of hexahydrite have been shown to slightly change depending on ambient conditions (UV radiation, CO_2 atmosphere and pressure) (Craig et al., 2006). A lot of work has been done to better understand the stability of hydrated Mg-sulfates in various physical conditions (Vaniman et al., 2004; Wang et al., 2006; Cloutis et al., 2007), to study the cycles of hydration-dehydration between the various phases $MgSO_4 \cdot nH_2O$ (Chou and Seal II, 2007), and to characterize the VNIR spectral behavior of large suites of sulfates with the goal of separating them (Crowley, 1991; Van Keulen et al., 2000; Cloutis et al., 2006). Reflectance spectra of several hydrated sulfates in the near infrared range have been studied at room and cryogenic temperatures (Dalton et al., 2005). In particular hexahydrite and epsomite have been measured at 300K and 100÷120K in the spectral range 0.3-2.5 μm by Dalton et al. (2005; 2012); hexahydrite spectra at 300K and 77K have been measured by McCord et al. (1999) in the range 0.9÷2.5 μm. Dalton et al. (2011) investigated hexahydrite spectra in the range 0.5-2.5 μm, in the temperature range 150-300K. Here we discuss the spectral behavior, in the extended visible and infrared range (0.5-4.0 μm), of hexahydrite and epsomite, considering a wide range of temperatures (93÷298K). Measurements have been performed at 8÷10 temperature steps in the above range and with three different grain sizes, in order to document the evolution of band parameters with temperature. From the summary hitherto presented, the investigation of hydrate sulfates in a spectral range comparable to remote sensing observation carried onboard ongoing and future interplanetary space missions is key to enforce the interpretation of those data. The presence of hydrated minerals, in particular mono- and poly-hydrated sulfates, in Solar System objects such as Mars and the icy Galilean satellites, requires detailed laboratory investigation of these materials in different environmental conditions. Hence a detailed spectral analysis of such minerals as a function of temperature is key to better understand and constrain future observations

2. Experiment and methods

2.1 Experimental setup

Measurements have been performed with the Spectro-Gonio-Radiometer facility (Brissaud et al, 2004) at the Institut de Planétologie et d'Astrophysique of Grenoble (IPAG). The instrument is a bidirectional VIS-NIR reflectance spectrometer; two detectors have been used to cover the 0.5-4.0 μm spectral range: a CCD in the 0.5-1.0 μm range and an IR detector in the 1.0-4.0 μm range. A monochromator was used as light dispersion element. Spectralon and Infragold (Labsphere ©) were used as commercial reference targets with an absolute calibration of the BRDF of Spectralon (Bonnefoy 2001). All spectra have been acquired with an illumination angle *i*=20° and an emission angle *e*=20°. The spectral resolution used in this setup is: 5 nm for λ=0.45-0.7 μm, 12 nm for λ=0.7-1.0 μm, 24 nm for λ=1.0-2.0 μm and 48 nm for λ=2.0-4.5 μm.

Measurements were carried out within the CARBONIR environmental chamber coupled with the spectro-gonio-radiometer (Grisolle 2013, Grisolle et al., 2014; Beck et al., 2015). This chamber is made of a large closed isothermal copper cell (diameter of 8 cm) inserted in a stainless steel chamber. The copper cell is cooled with a He-cryostat and optical access is permitted through sapphire windows. This setup enables measurement of reflectance spectra at temperatures down to 50 K. In order to ensure efficient thermal coupling of the sample, a few mbar (monitored during the experiment) of dry air were kept in the cell. The cell temperature is monitored during the experiment and the error on sample temperature is estimated to be of the order of 1 K.

2.2 Samples

Two sulfate samples have been analyzed. Hexahydrite ($MgSO_4 \cdot 6H_2O$), which is hexa-hydrated magnesium sulfate, and epsomite ($MgSO_4 \cdot 7H_2O$), which is epta-hydrated magnesium sulfate. Each sample has been grinded from coarser grains and dry-sieved by shaking in three different grain sizes: 20-50 μm, 75-100 μm and 125-150 μm. The grain sizes have been chosen in order to avoid overlapping between ranges, so as to minimize particles contamination among the dimensional classes.

2.3 Reflectance measurements

Spectra have been acquired for each grain size at different temperatures (Figs. 1,2,3). The whole temperature range covers 93 K ÷ 298 K. Measurements have been performed at steps of 10÷15K in the low temperature range, and at steps of 20÷25 K in the high temperature range, for a total of 8÷10 steps on average for each grain size. All samples have been analyzed starting at the lowest temperature (T_0 = 93 K) and then acquiring subsequent spectra during the rise of *T* up to 298 K.

All the band parameters have been computed after removing the spectral continuum (Figs. 4a,b,c): for each band a straight line has been drawn between the band edges, by intersecting the

visually identified maxima of both band extremes, and then removed by dividing the spectrum by this line. The band center is determined by applying a second-order polynomial fit around the band minimum, and taking the resulting minimum of the fit as the band center value. The depth is computed, following Clark and Roush (1984), as $D=(R_C-R_B)/R_C$, where R_B and R_C are the reflectance of the band and the spectral continuum at the band center, respectively. The width has been computed by intersecting the continuum-removed band with a horizontal line passing through half depth. In the case of multi-peak bands (Fig. 4b), the continuum line for background removal is drawn between the edges of the whole band, and each single peak is fitted with second-order polynomials. The 3-μm feature, as schematized in Fig. 4c, is very asymmetric, and is indeed due to the overlapping of two absorptions, a narrow one centered at 2.7 μm (O-H stretching) and a much broader one centered near 3 μm (overtone of H-O-H bending occurring near 6 μm) [Clark et al., 1990]. We decided to focus on the 3-μm absorption and modeled the minimum with a second-order polynomial, because of high instrumental noise around 2.7 μm. It should be noted that, in principle, the whole band could be fitted by the sum of two Gaussians, with higher spectral resolution and higher signal-to-noise data.

3. Results: spectral parameters analysis

3.1 Spectral variability

Measured spectra are shown in Fig. 1 (hexahydrite) and Fig. 2 (epsomite). The spectra of these hydrated minerals are very similar in the overall profile, although several subtle differences arise when looking at the absorption bands in detail. A test was performed by measuring a given sample (hexahydrite, 125-150 μm) both during the temperature-increasing and the decreasing phase: no major changes have been observed neither in the spectral profiles nor in the band positions (Fig. 3). Spectra of both hexahydrite and epsomite are characterized by several absorption bands in the range 1.0÷3.7 μm. The main features are centered at 1.0, 1.2, 1.35, 1.5, 1.9, 2.2, 2.5, 2.7 and 3.0 μm. Essentially all these features are due to transitions in O-H groups and in H_2O molecules. The bands at 1.0, 1.2, 1.35, 1.5 are overtones and combinations of the stretching fundamental transition in OH groups present in the crystal lattice, occurring near 2.75 μm (Hunt, 1977; Clark et al., 1990; Dalton et al., 2005).

The features near 1.9 and 3.0 μm are due to O-H stretching and H-O-H bending vibrations in the H_2O molecule. The fundamental modes of these transitions occur near 2.9, 3 and 6 μm, and overtones and combinations are observable in the VNIR range near 0.94, 1.14, 1.38, 1.45 and 1.9 μm (Hunt, 1977; Clark et al., 1990). Association of SO_4^{2-} groups and H_2O molecules could be responsible of the features appearing at 2.2 μm (in hexahydrite) and 2.5 μm (in both samples) (Gendrin et al., 2005; Cloutis et al., 2006) rather than metal-OH bond vibrations (Hunt, 1977; Clark et al., 1990; Clark, 1999). Bending and stretching vibrations in S-O groups could be observed here, because overtones of fundamental vibration modes occurring in the 8-24 μm region are expected

in the 4-5 μm region and in the 2.1-2.7 μm region, which falls within our range of sensitivity (Cloutis et al., 2006).

According to Cloutis et al. (2006), the absorption feature at 2.55 μm could be related to OH/H_2O content. The OH band in the 1.5-μm region is broad and has edges at 1.3 and 1.8 μm approximately. In the case of hexahydrite ($6 \cdot H_2O$), the fine structure of the band is constitued by a triplet that becomes more and more defined as temperature decreases. The first two features of the triplet occur at 1.47 and 1.55 μm; the third is weak (with a width of about 20 nm) and is visible only at very low temperatures, therefore it has not been considered here. At higher temperatures only the band centered at 1.47 μm is evident. In the case of epsomite ($7 \cdot H_2O$), this band is constitued by a doublet; the two absorptions centered at 1.5 and 1.62 μm become more and more resolved as temperature drops down, and the feature at 1.62 μm tends to have a nearly flat base; a higher spectral resolution would be needed to properly discern the band structure. The water band at 3 micron is very broad and almost saturates the absorption; its wings extend up to 3.7 μm in the infrared region. The long-wavelength edge of the band tends to become unrecognizable especially for coarser grain sizes and at higher temperatures, as shown for example by the spectrum of hexahydrite 125-150 μm at 298 K (Fig. 1). In spectra of epsomite (Fig. 2) the long-wavelength edge of the 3-micron band completely disappears for grain sizes 75-100 and 125-150 μm, at temperatures higher than 203 K.

Hexahydrite								
T (K)	*Absorption features (μm)*							
298	1.0	1.2	1.5					
93	1.0	1.2	1.35	1.47	1.55	1.61	1.68	1.77
298	2.0					2.2	3.0	
93	1.94	1.98	2.01	2.06	2.12	2.2	2.5	2.7	3.0
Epsomite								
T (K)	*Absorption features (μm)*							
298	1.0	1.2	1.5					
93	1.0	1.2	1.4	1.5	1.62	1.66	1.78	
298	2.0			3.0				
93	1.95	2.0	2.06	2.5	2.7	3.0		

Tab.1. Absorption features at room (298K) and cryogenic (93K) temperature.

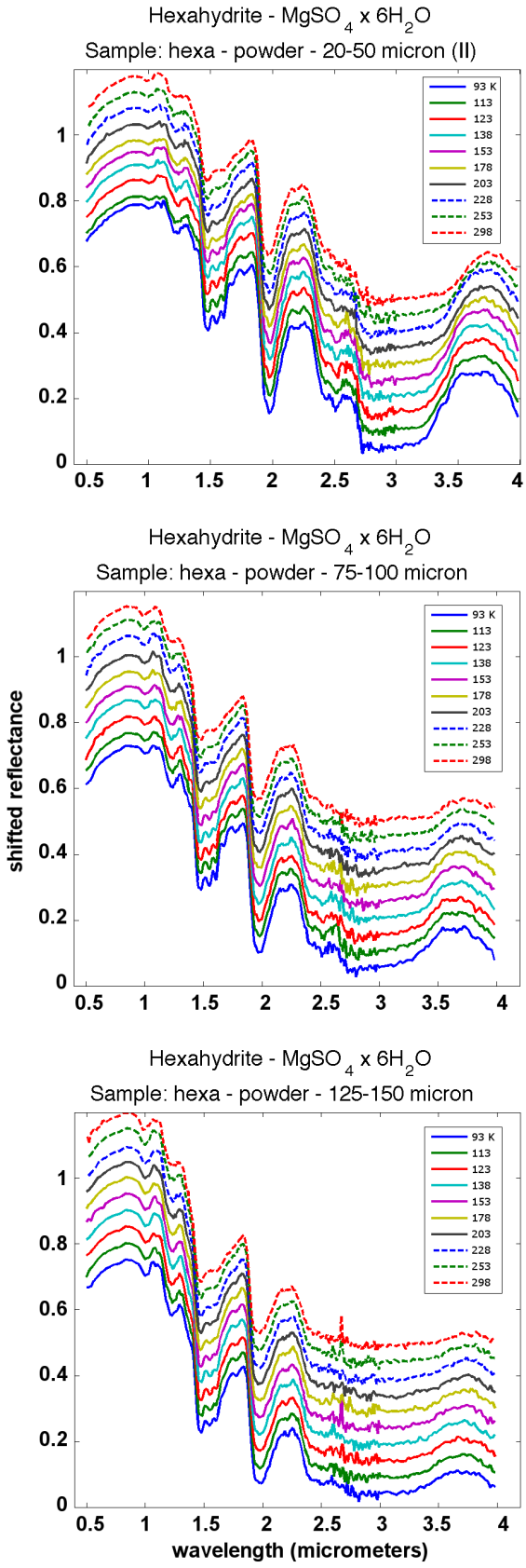

Fig.1. Spectra of hexahydrite at different temperatures, in the range 93 ÷ 298K. Top: grain size 20-50 μm. Center: grain size 75-100 μm. Bottom: grain size 125-150 μm. Above 93K spectra are up-shifted in reflectance by 0.05 for clarity.

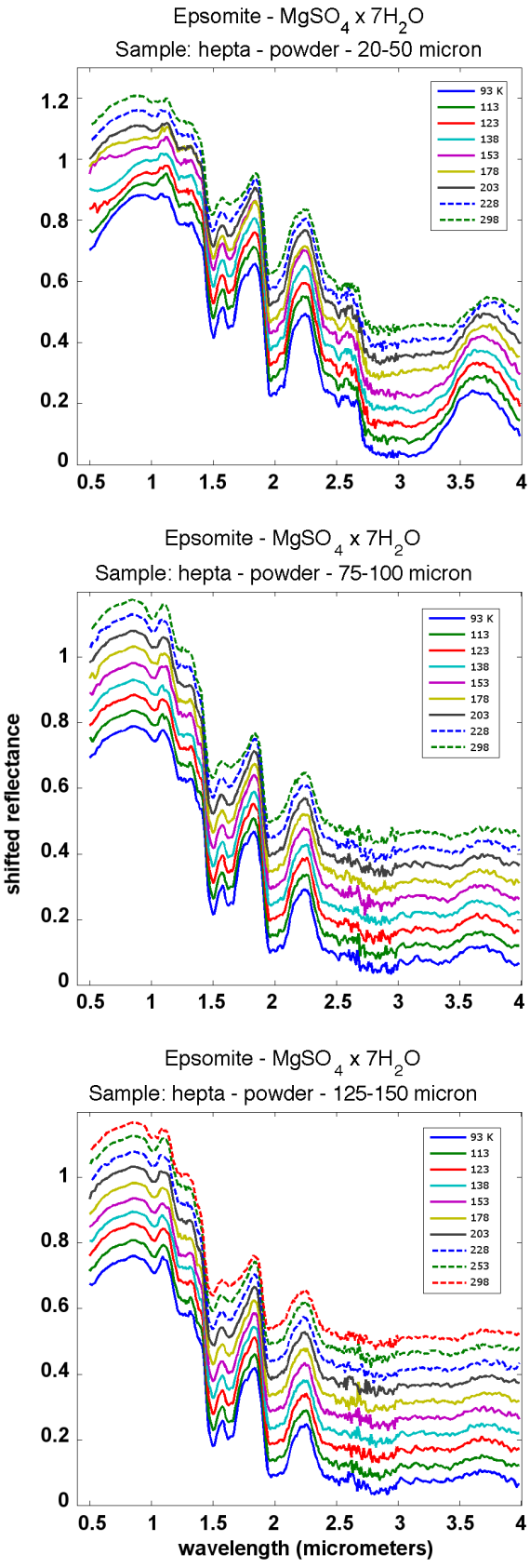

211

212 *Fig.2. Spectra of epsomite at different temperatures, in the range 93 ÷ 298K. Top: grain size 20-50 μm.*
213 *Center: grain size 75-100 μm. Bottom: grain size 125-150 μm. Spectra above 93K are up-shifted in*
214 *reflectance of 0.05 for clarity.*

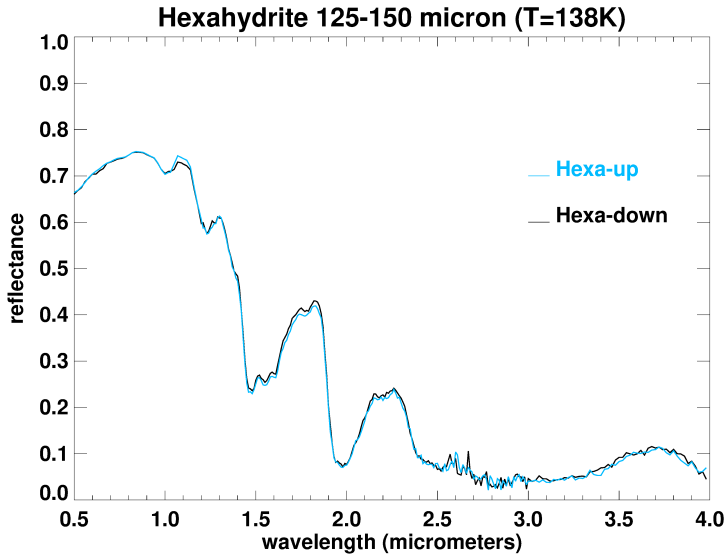

Fig.3. Spectra of hexahydrite (125-150 μm) at T=138K. The cyan ("up") spectrum has been acquired during the temperature-increase phase of measurements; the black ("down") spectrum has been acquired during the temperature-decrease phase. The spectral profiles do not show variations.

3.2 Spectral parameters analysis

Different absorption bands have been analyzed for each spectrum of the two samples, in the entire range of explored temperatures (Fig. 4a). Band parameters such as position, area, depth and width have been determined (Fig. 4b,c). Thus for each sample and each grain size, the band parameters have been studied as a function of temperature. Depending on the particular analyzed absorption feature, for some values of temperature it was not possible to retrieve some of the parameters. All parameters were computed after removal of the spectral continuum, as described in Section 2.3.

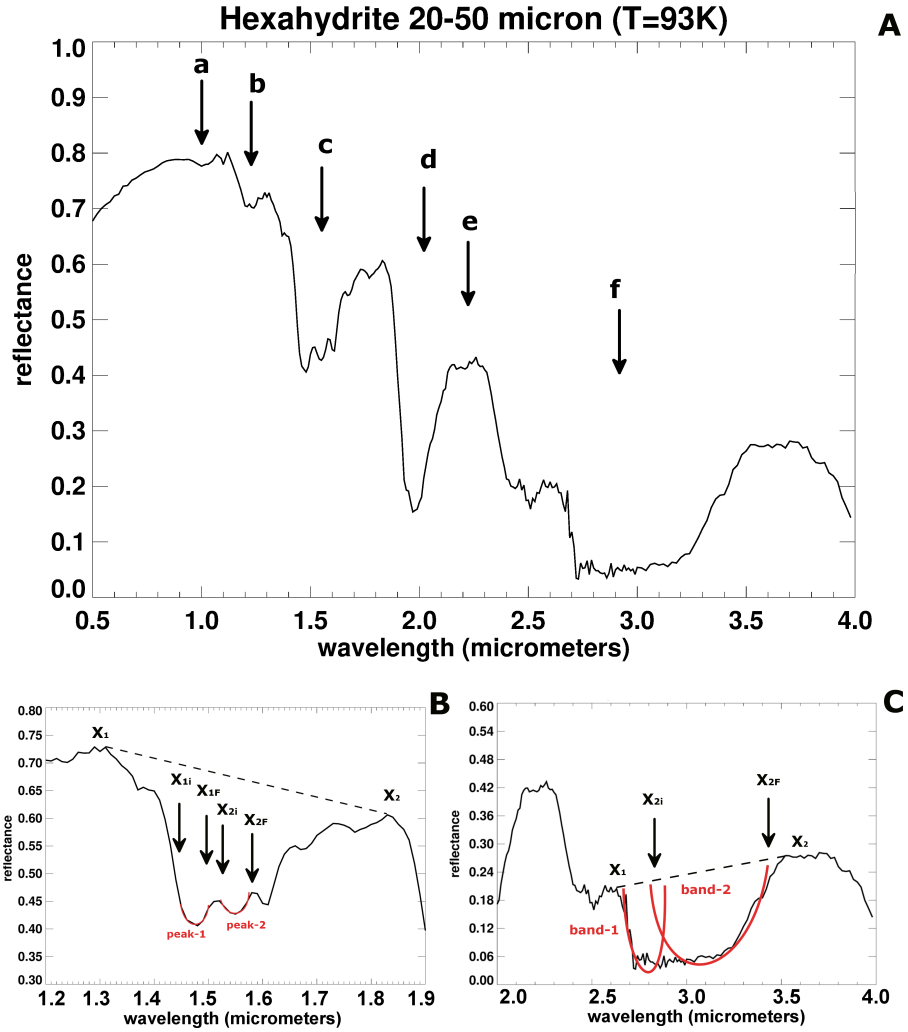

Fig.4. A: absorption bands analyzed in the spectra of the two samples. Band a: 1 μm. Band b: 1.2 μm. Band c: 1.5 μm. Band d: 2 μm. Band e: 2.2 μm. Band f: 3 μm. B: method of band fitting for multi-peak bands. In the case of the broad 1.5-μm feature, the continuum baseline has been drawn between the points X_1, X_2. After continuum removal by division, the two minima at 1.47 (peak-1) and 1.55 μm (peak-2) have been fitted with 2nd order polynomials between two extremes X_{1i}-X_{1F} and X_{2i}-X_{2F}, respectively. Bands have been resampled with 10^3 points before polynomial fitting. The area is computed between X1-X2 and so refers to the area of whole band. C: fitting of the 3-μm band. The edges X_1,X_2 for continuum removal have been put at 2.6 and 3.54 μm, while the 2nd order polynomial has been computed, after a denser resampling, between X_{2i},X_{2F} = 3, 3.42 μm. Band edges X_1,X_2 and X_{2i},X_{2F} have been chosen appropriately for each analyzed band and each spectrum, and not kept constant for all dataset, in order to take into account variations from one spectrum to another (i.e. variations with temperature and grain size).

3.3 Hexahydrite

1-micron band.

This band is weak but well defined for each size and temperature (Fig. 1). The absorption's intensity, as well as depth, clearly changes with changing grain size (Figs. 1, 5), whereas for a given grain size there is no trend with temperature (Fig.5b). The position (center) of the absorption (Fig.5a) varies within a narrow range (0.99 to 1.01 μm) and shows a shift towards longer wavelengths with decreasing temperature. The band depth (Fig. 5b) shows a behavior compatible with the absorption area (Fig. 5c). The width of the absorption varies within 0.08 and 0.10 μm and no trend is observed as a function of size or temperature (Fig. 5d).

1.2-micron band.

The second absorption is located inside the shoulder of the strong 1.5 H_2O band. At our spectral resolution this feature is weak, asymmetric, with a less defined minimum for the 20-50 μm size fraction and at the highest temperature for the other sizes (Fig. 1). Moreover at low temperature we have indication of possible absorptions with finer structure, resolvable at higher spectral resolutions. The position of the absorption (Fig. 6a) varies within a narrow range (from 1.20 to 1.22 μm) with decreasing temperature. This shift is almost linear for the 75-100 μm size, whereas the other two sizes show a similar trend but only until *T*=173-138K, while at lower temperatures the position moves back towards 1.21 μm. This is probably related to the appearance of a new weak minimum within the 1.22-1.23 μm range, not well resolvable at the considered spectral resolution. The absorption depth slightly increases with the size and inversely with temperature (Fig. 6b). The band area also increases directly with the size, and inversely with temperature (Fig. 6c). The width (FWHM) is 0.10 μm and no trend is observed as a function of size or temperature (Fig. 6d).

1.5-micron band.

The OH absorption band at ~1.5 μm is actually due to a combination of three weaker features centered at 1.47, 1.55, and 1.61 μm, respectively. This band appears as a triplet only at cryogenic temperatures, while it is a doublet at ambient temperature. Concerning the 1.47 μm feature, all four parameters have been computed for the three grain sizes; the trends are shown in Fig. 7. The band position (fig.7a) slightly shifts towards longer wavelengths as the temperature decreases. The depth increases substantially as the temperature decreases (fig.7b). The band area (fig.7c) tends to greater values towards lower temperatures. The band gets narrower (fig.7d).

Regarding the 1.55 μm band, all parameters were computed: position, depth, area and width (Fig. 8). The position of this feature (Fig. 8a) was computed for temperatures below 223 K, and no significant trend is evident. The depth shows a strong dependence with temperature: again the depth increases with decreasing temperature (Fig. 8b). Both area (Fig.8c) and width (Fig. 8d) show an overall dependence with temperature, with a general increase towards lower *T* values, although these two parameters are quite constant in the range *T*=113÷173K. Band centers at 1.47 and 1.55 μm seem to be correlated. The 1.61-μm feature is very weak and only shows up at very low temperatures, i.e. below 173 K. At higher temperatures, this feature and the central feature at 1.55 μm merge together. As temperature raises up to room values, the 1.55-μm band becomes hardly recognizable and only the feature at 1.47 μm remains detectable (see Discussion in Section 4). Band parameters for the 1.61-μm feature have not been computed in this analysis.

1.9-micron band.

The band parameters computed for the water band at 1.9 μm are shown in Fig. 9. The band center (fig.9a) shifts towards longer wavelengths from about 1.95 μm to 1.97 μm when cooling from room temperature down to 93K. Both the band depth (Fig. 9b) and band area (Fig. 9c) show an increase towards lower temperatures. No significant temperature dependence has been retrieved for the band width (Fig. 9d).

2.2-micron band.

The trends are shown in Fig. 10. While the band center (Fig. 10a) does not show any particular trend, band depth and band area display a correlation with changing temperature. Both depth (Fig. 10b) and area (Fig. 10c) become greater as the temperature decreases. This weak band becomes even more evident and recognizable at very low temperatures. Band width (fig.10d) gets greater at low T at least for the grain sizes 20-50 and 75-100 μm.

3-micron band.

This band is related to a combination of transitions in OH^- and H_2O (Cloutis et al., 2006). Position, depth and area show neat correlation with the temperature variation (Fig. 11): as the temperature decreases, the band position (Fig. 11a) shifts towards shorter wavelengths in the range 3.0-3.1 μm, for the grain sizes 20-50 and 75-100 μm. Conversely, the band position of coarser grain size (125-150 μm) does not show any obvious correlation with temperature. Its depth increases with decreasing temperature (Fig. 11b); moreover the fine powder shows the largest values of band depth, while the coarse powder shows the smallest values of depth; the medium powder showing intermediate values. The water band area (Fig. 11c) tends to decrease as the temperature drops

down, for all the analyzed grain sizes. The band width (Fig. 11d) appears to get smaller as T decreases.

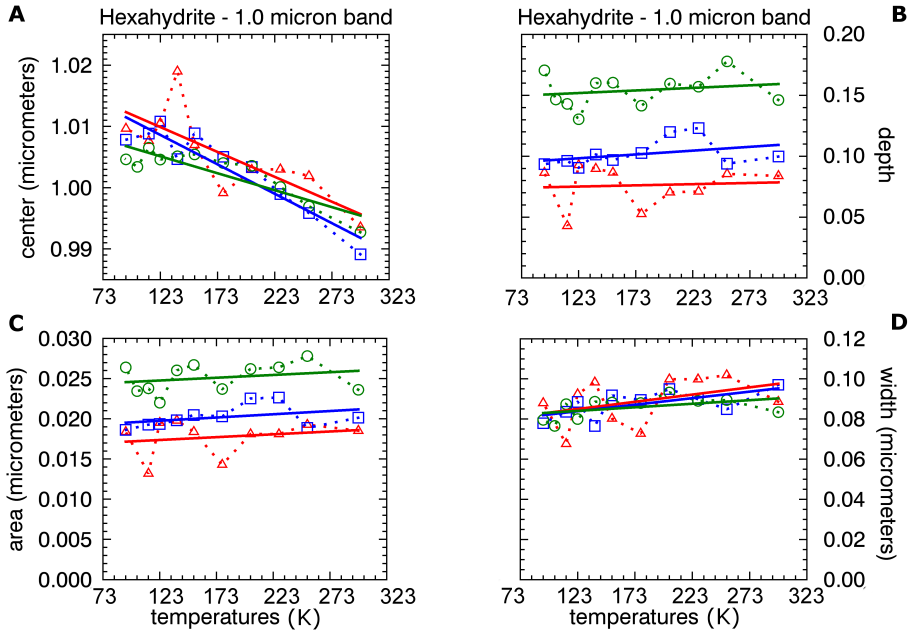

Fig.5. Band parameters determined for the band at 1.0 μm, hexahydrite. Red triangles: grain size 20-50 μm. Blue squares: 75-100 μm. Green circles: 125-150 μm.

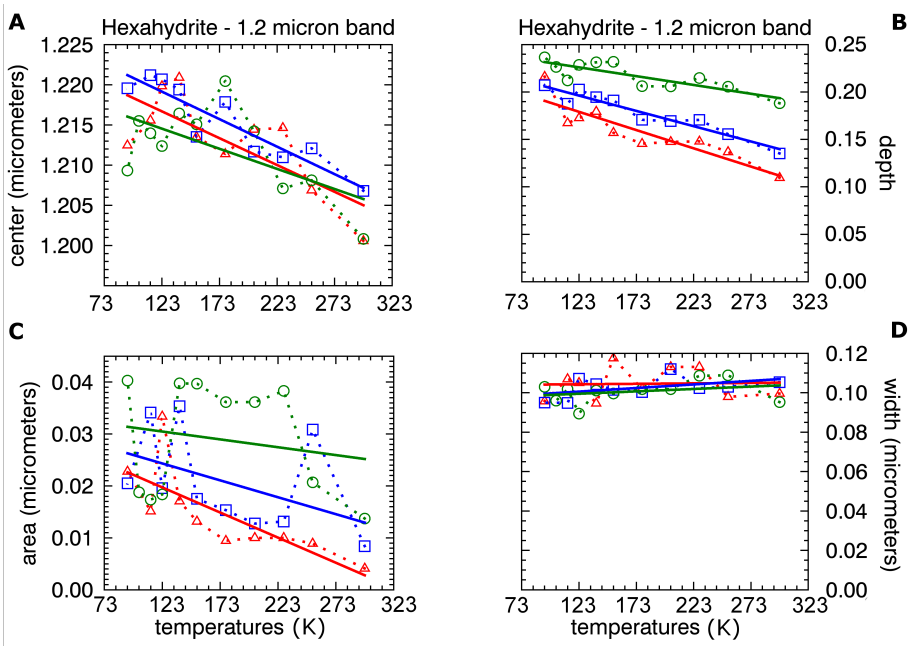

Fig.6. Band parameters determined for the band at 1.2 μm, hexahydrite. Red triangles: grain size 20-50 μm. Blue squares: 75-100 μm. Green circles: 125-150 μm.

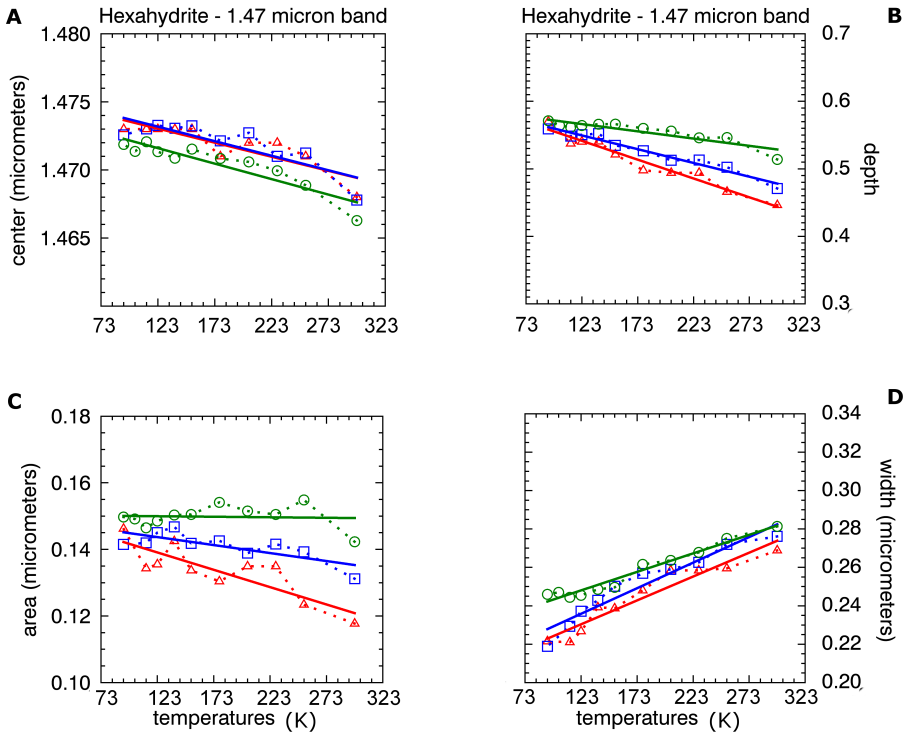

Fig.7. Band parameters determined for the band at 1.47 μm, hexahydrite. Red triangles: grain size 20-50 μm. Blue squares: 75-100 μm. Green circles: 125-150 μm.

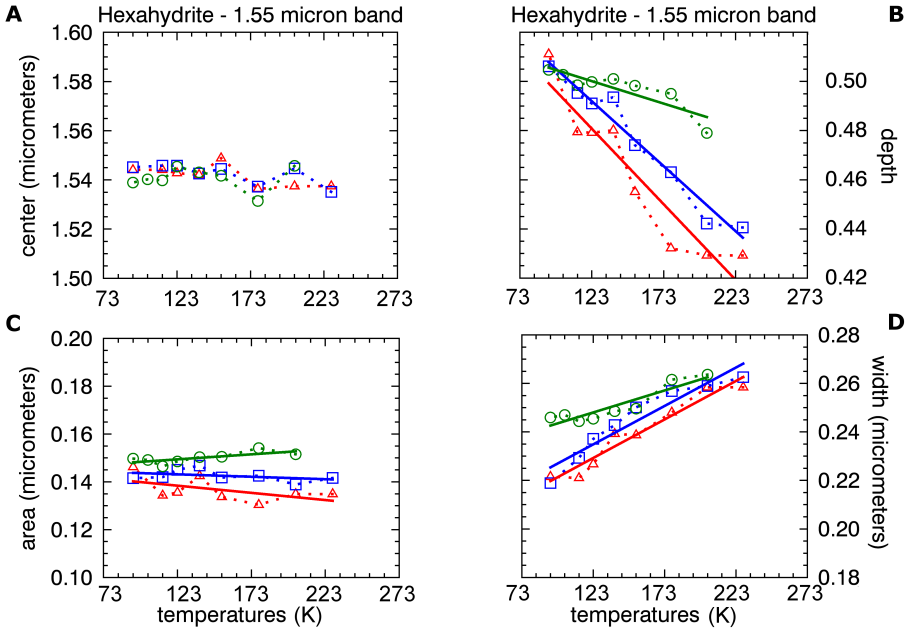

Fig.8. Band parameters determined for the band at 1.55 μm, hexahydrite. Red triangles: grain size 20-50 μm. Blue squares: 75-100 μm. Green circles: 125-150 μm.

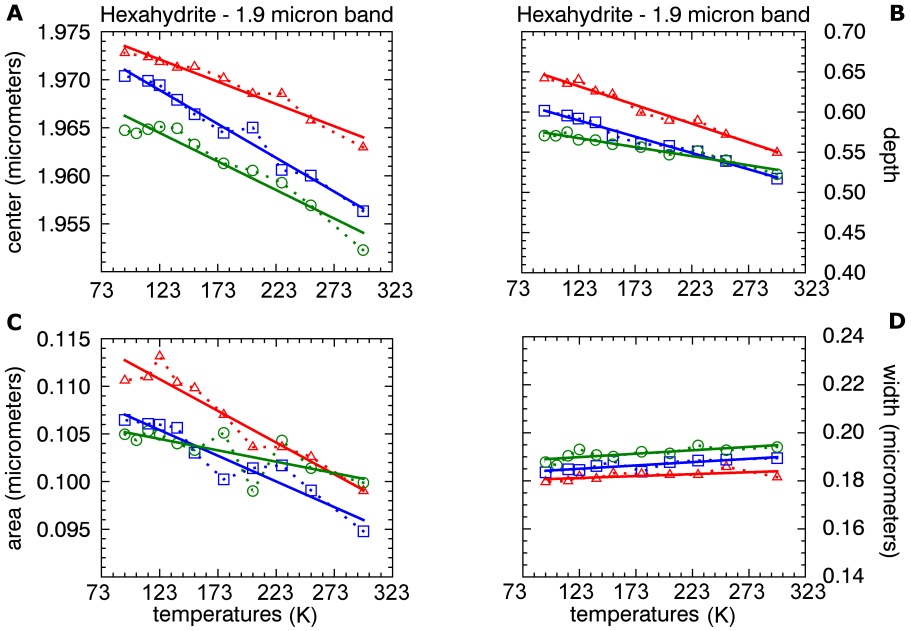

Fig.9. Band parameters determined for the band at 1.9 μm, hexahydrite. Red triangles: grain size 20-50 μm. Blue squares: 75-100 μm. Green circles: 125-150 μm.

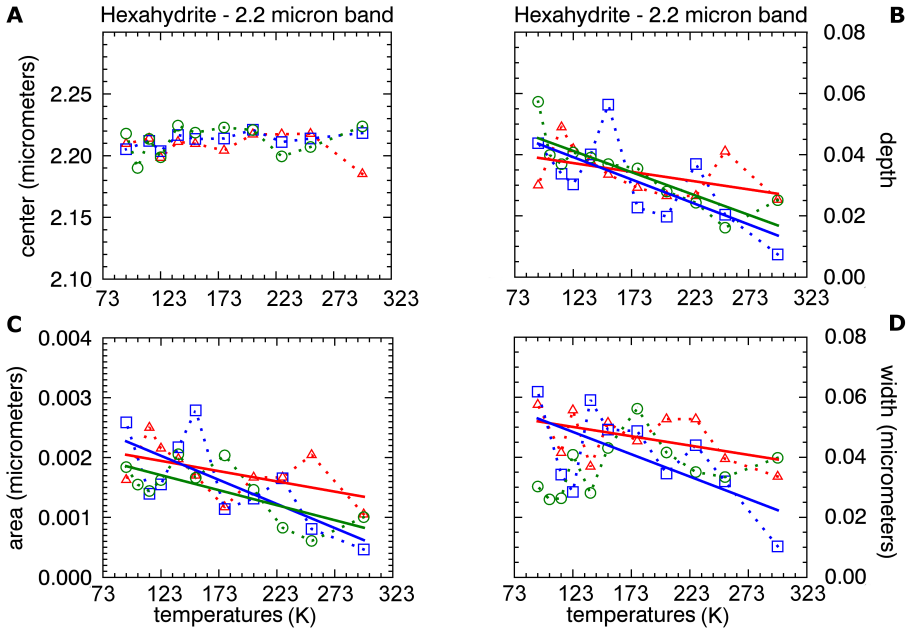

Fig.10. Band parameters determined for the band at 2.2 μm, hexahydrite. Red triangles: grain size 20-50 μm. Blue squares: 75-100 μm. Green circles: 125-150 μm.

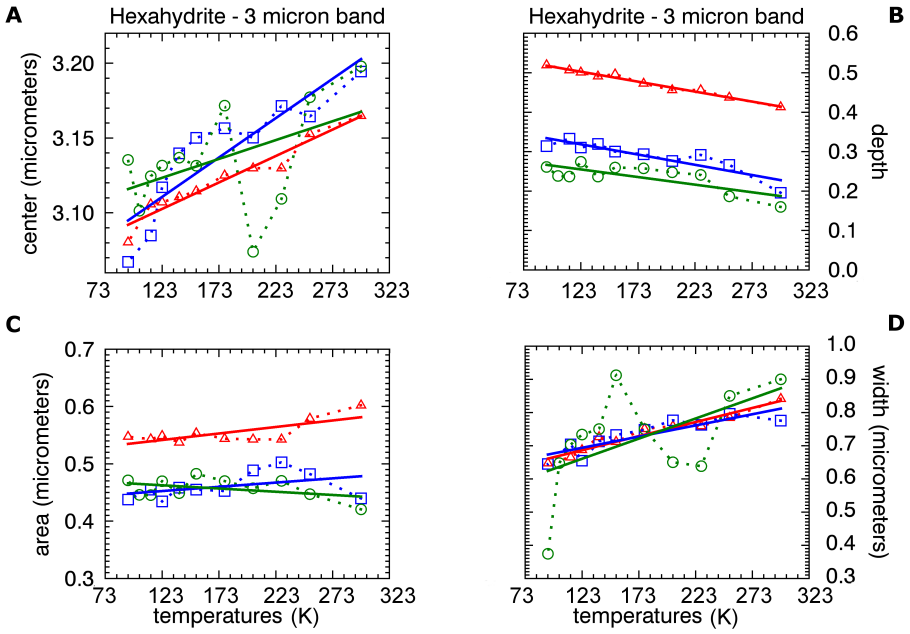

Fig.11. Band parameters determined for the band at 3 μm, hexahydrite. Red triangles: grain size 20-50 μm. Blue squares: 75-100 μm. Green circles: 125-150 μm.

3.4 Epsomite

1-micron band.

Also for epsomite this band is weak, but well defined for each grain size and temperature (Fig. 2). The absorption's center (Fig.12a) varies within 1.00 and 1.03 μm, showing a shift with temperature. As well as for hexahydrite, the position moves to longer wavelengths with decreasing temperature. This trend is almost linear for 75-100 and 125-150 μm, whereas for the smallest size it shows a steep variation between 223 and 173K. The strong asymmetry seen for lower temperatures could suggest a possible shift towards longer wavelengths, if the absorption could be sampled at higher spectral resolution. The absorption intensity, as both depth and area, slightly varies within narrow ranges without defined trends with size and temperature (Fig.12b,c). The width (FWHM) of absorption is around 0.9 μm (Fig.12d).

1.2-micron band.

This absorption takes place inside the strong 1.5-μm H_2O absorption, and a defined band is actually observed only for the 120-150 μm size. Lower sizes show a bent, with the possible presence of relative minima, not resolved with our setup. For the 120-150 μm size the absorption is weak and asymmetric (Fig. 2). The position of the absorption (Fig. 13a) slightly varies from 1.21 to 1.22 μm with decreasing temperature. A finer structure across the band minimum is outlined but not well resolvable. The absorption depth slightly increases with grain size and inversely with

374 temperature (Fig.13b), whereas the band area shifts around 0.02 (Fig. 13c). The band width is 0.10
375 μm (Fig.13d).

376

377 *1.5-micron band*.

378 Like hexahydrite, epsomite shows a prominent OH^- band centered near 1.5 μm, which in this case
379 is the combination of a doublet of absorptions, centered at about 1.5 and 1.62 μm. These two
380 signatures become more distinctly resolvable as the temperature decreases. The parameters
381 computed for the 1.5-μm feature are shown in Fig. 14. This band center (Fig. 14a) shifts towards
382 longer wavelengths in the range 1.48-1.50 μm as the temperature decreases. Band depth (Fig.
383 14b) and band area (Fig. 14c) show similar trends: both become larger as the temperature
384 decreases. The width becomes narrower towards lower values of temperature (Fig. 14d).

385 The parameters of the secondary feature at 1.62 μm are shown in Fig. 15. All the parameters are
386 characterized by monotonous trends, similar to those related to the 1.5-μm signature. The band
387 center (Fig. 15a) shifts towards longer wavelengths in the range 1.59-1.63 μm as the temperature
388 decreases down to 93 K. Again, band depth and band area (Fig. 15b,c) show an increase as the
389 temperature decreases. Similar to the 1.5-μm feature, the 1.62-μm feature is characterized by a
390 width that becomes narrower as the temperature decreases (Fig. 15d).

391

392 *1.9-micron band*.

393 The parameters relative to the H_2O absorption band are displayed in Fig. 16. They show an evident
394 correlation with temperature, except for the width. The band center (Fig. 16a) shifts towards
395 longer wavelengths in the range 1.96-1.98 μm as the temperature decreases. Band depth and area
396 (Fig. 16b,c) are both characterized by an increase towards lower values of temperature. The width
397 shows no trend (fig.16d).

398

399 *3-micron band*.

400 The prominent water absorption feature centered at approximately 3 μm is difficult to analyze for
401 grain sizes 75-100 μm and 125-150 μm, because saturation affects the spectra above 2.3 μm. Thus
402 the 3-μm feature has been only analyzed for the grain size 20-50 μm (Fig. 17). The left and right
403 shoulders of the band have been chosen near 2.6 and 3.7 μm, respectively. With a shoulder taken
404 at 2.6 μm, a band centered near 2.5 μm shows up. But this is only evident for 20-50 μm grain size,
405 and it has not been considered here. As for the hexahydrite, the band position (Fig. 17a) shifts
406 towards shorter wavelengths as the temperature decreases, in the range 3.04-3.12 μm. The band
407 depth (Fig. 17b) is characterized by a strong increasing trend while the temperature drops down.

Both the band area (Fig. 17c) and the band width (Fig. 17d) are characterized by decreasing trends going towards lower values of temperature.

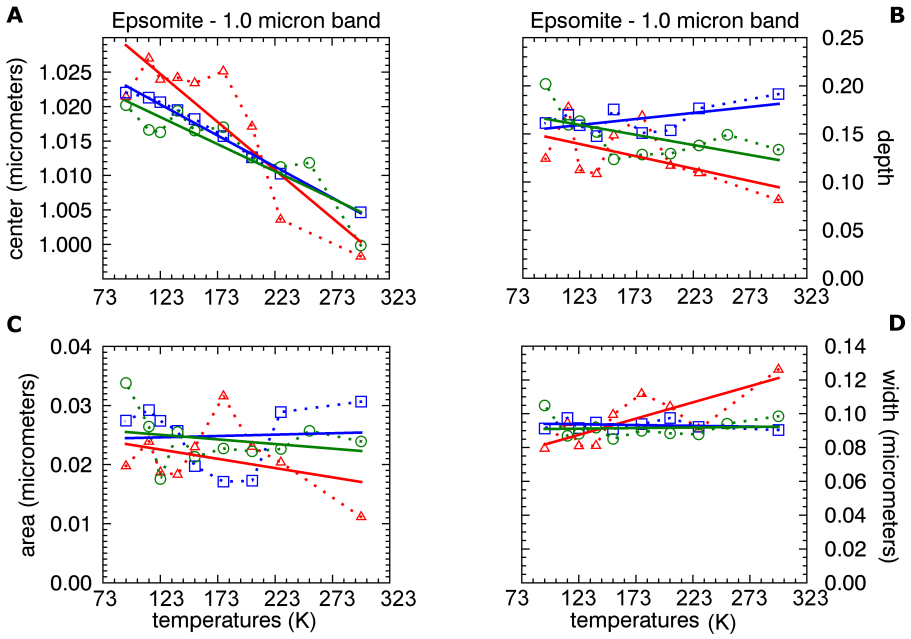

Fig.12. Band parameters determined for the band at 1.0 μm, epsomite. Red triangles: grain size 20-50 μm. Blue squares: 75-100 μm. Green circles: 125-150 μm.

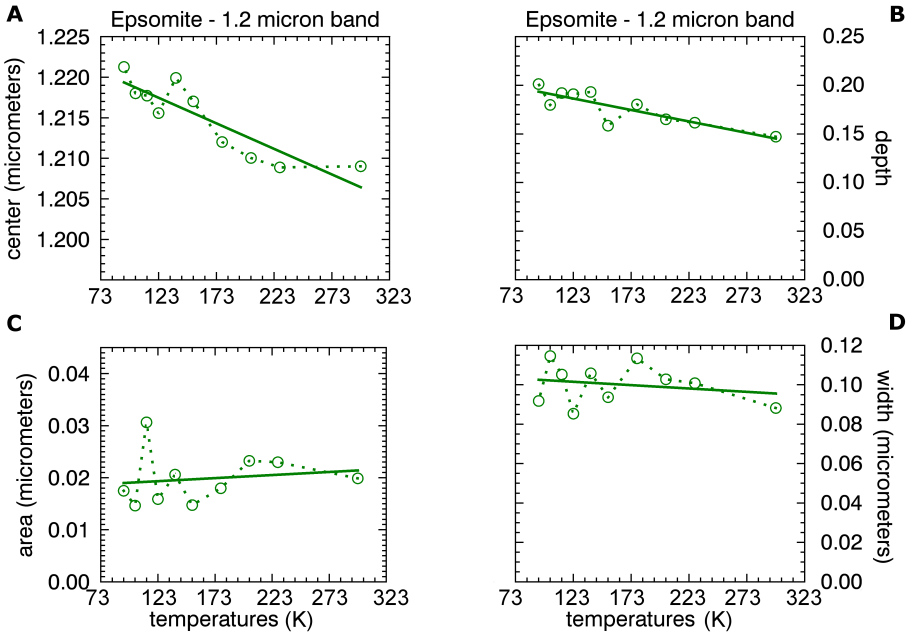

Fig.13. Band parameters determined for the band at 1.2 μm, epsomite. Green circles: 125-150 μm.

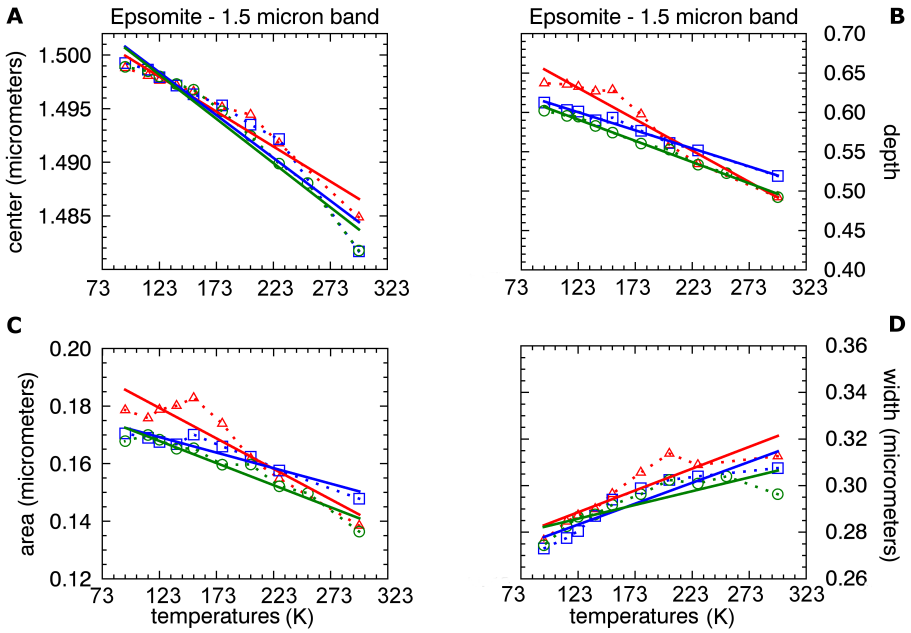

Fig.14. Band parameters determined for the band at 1.5 μm, epsomite. Red triangles: grain size 20-50 μm. Blue squares: 75-100 μm. Green circles: 125-150 μm.

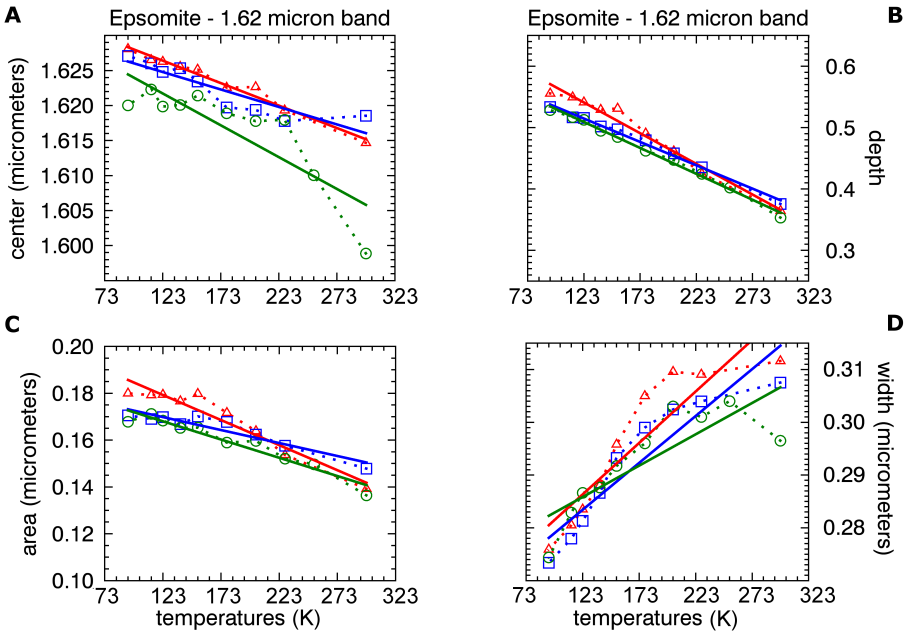

Fig.15. Band parameters determined for the band at 1.62 μm, epsomite. Red triangles: grain size 20-50 μm. Blue squares: 75-100 μm. Green circles: 125-150 μm.

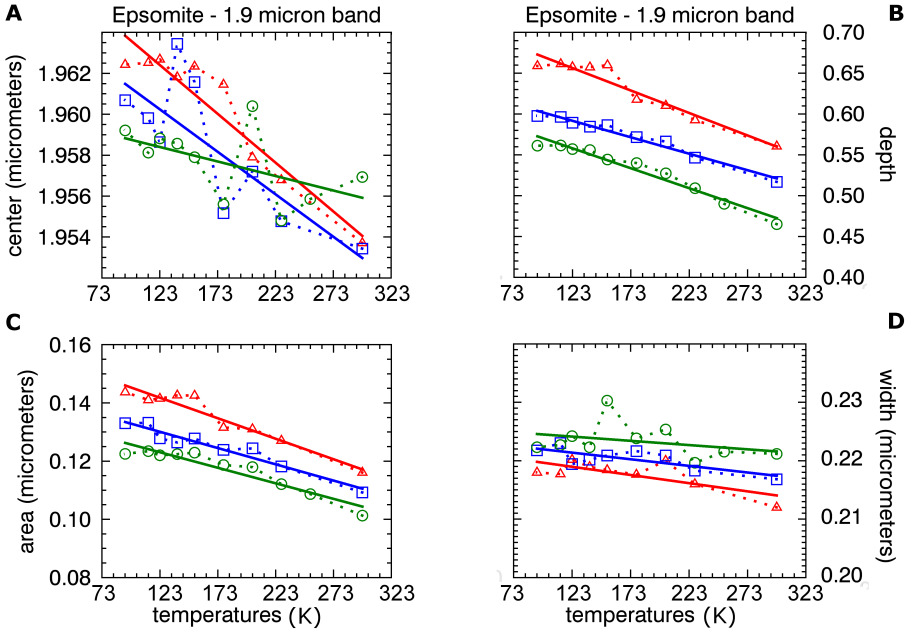

Fig.16. Band parameters determined for the band at 1.9 μm, epsomite. Red triangles: grain size 20-50 μm. Blue squares: 75-100 μm. Green circles: 125-150 μm.

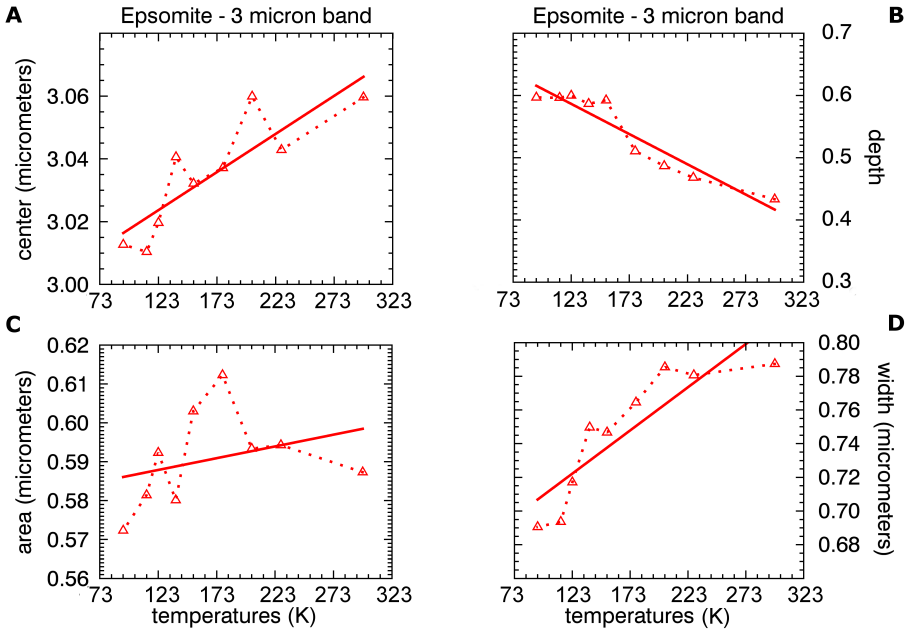

Fig.17. Band parameters determined for the band at 3 μm, epsomite. Red triangles: grain size 20-50 μm.

4. Discussion

Hexahydrite and epsomite spectra show overtone absorptions in similar spectral ranges but some differences are visible. The most evident variation is in the H-O-H/O-H bands near 1.5 μm (Figs. 1,2 and Fig.18a), and the other two most different absorptions are those related to H_2O, in particular the 1.9/2 μm feature (Fig. 19).

Hexahydrite vs Epsomite at 1.5 μm

Hexahydrite's 1.5-μm absorption shows a triplet/three minima profile, which becomes more and more evident as the sample is cooled down to 93 K (Fig.18a), whereas epsomite's 1.5-μm signature has a doublet/two minima shape (Fig. 18b) at all temperatures. At room temperature, hexahydrite feature becomes a broad band with a single minimum centered at about 1.47 μm.

In the fine structure of the whole absorption band (between 1.32 and 1.83 μm) for spectra acquired at low temperature for both samples, we can discern three additional weak features. These can be recognized at the spectral resolution of about 24 nm in this range (see section 2.1).

McCord et al. (1999) pointed out that the fine structure of hexahydrite spectrum at 77 K consists of six absorption features, as measured in laboratory at a spectral resolution of 10 nm. In their study, McCord et al. (1999) suggested that the number of absorption transitions, in the H-O-H/O-H feature fine structure at 1.5 μm, could be proportional to each site in the mineral crystal structure occupied by a water molecule. However, Cloutis et al. (2006) reported the existence of two minima centered at 1.44 and 1.46 μm within the fine structure of hexahydrite's 1.5-μm band as measured at room temperature, stating that all these signatures are H_2O overtones/combinations. They also interpret small minima in the fine structure of bands occurring in the 1.4-1.5-μm region in other sulfates as related to OH^- or H_2O overtones and combinations (Cloutis et al., 2006). Dalton et al. (2005) and Dalton and Pitman (2012) refer to the band in the 1.4-1.6-μm region of hexahydrite/epsomite as related to O-H stretching overtones. The fine structure of these features, as observed at cryogenic temperatures, could be related to OH^- groups occupying different locations in the crystal lattice (Dalton et al., 2005, and references therein).

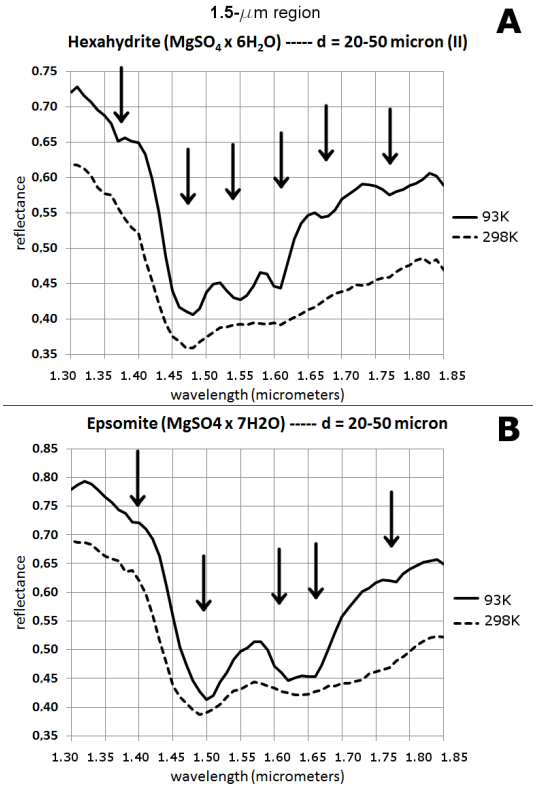

Fig.18. OH absorption band at 1.5 μm. A: hexahydrite. B: epsomite. For each sample, the line-curve is at 93K, while the dashed curve is at room temperature (shifted for clarity).

Hexahydrite vs Epsomite at 2 μm

Prominent differences between hexahydrite and eposmite are those related to H_2O, in particular the 1.9/2 μm feature (Fig. 19). This absorption shows a better defined V-shape with a clear minimum for all temperatures and all sizes in hexahydrite (Fig. 19a), whereas epsomite shows a less defined minimum (Fig. 19b). This absorption is probably characterized by several minima at low temperature, even though our spectral resolution did not allow us to unambiguously resolve them. The 3-μm band is well defined for smaller sizes and lower temperatures, but it is still detectable also for the other sizes (75-100 μm and 125-150 μm) in hexahydrite spectra. Conversely, epsomite shows a saturated plateau at wavelength > 2.3 μm for coarser grain sizes, because it contains more water (Figs. 1,2).

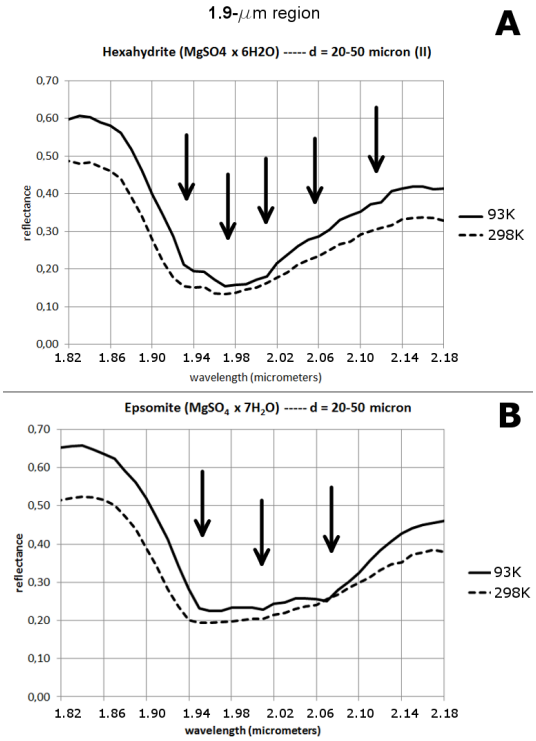

Fig.19. H_2O absorption band at 1.9 μm. A: hexahydrite. B: epsomite. For each sample, the line-curve is at 93K, while the dashed curve is at room temperature (shifted for clarity).

Band ratio at 1.5 μm

We have investigated the relative strengths of individual minima constituting the hexahydrite triplet and the epsomite doublet. The ratio of 1.47 to 1.55 μm band depths in hexahydrite has an evident increasing profile with increasing temperature (Fig. 20a): at cryogenic temperatures, the 1.55 μm band becomes clearer and more prominent, while at room temperature the 1.47 μm band is dominant. Similarly, in Fig. 20b the depth ratio 1.50-μm / 1.62-μm is shown. A similar trend shows up for all of the three grain sizes, as already mentioned for the analogous band of hexahydrite. The depth ratio decreases in a monotonous manner as the temperature decreases: at high temperatures the 1.5-μm feature is predominant, while at low temperatures the 1.62-μm minimum becomes important and comparable with the former one. The increasing separation, narrowing and definition of these bands occurring towards cryogenic temperatures is attributed to a decreasing thermal agitation of the molecular species in the mineral structure; the distribution of intermolecular couplings narrows and discrete absorption bands arise from both decreasing width and increasing peak intensity of closely spaced bands (Dalton et al., 2005). At the same time as the number of water molecules in the structure increases, the absorption bands tend to be larger and broader, due to the increased range of transition energies and probabilities with enhanced number of molecular vibrations combinations (McCord et al., 1999; Dalton et al., 2005).

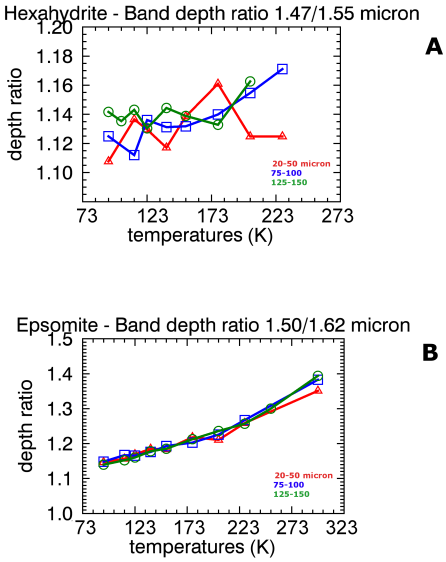

Fig.20. A: depth ratio for the bands at 1.47 and 1.55 μm (hexahydrite). B: depth ratio for the bands at 1.50 and 1.62 μm (epsomite).

Band position of water 3-μm band vs other features

Concerning band positions, different behaviors are observed if we consider the water band at 3 μm or the other features. Indeed, in both hexahydrite and epsomite, the 3-μm band position shifts towards shorter wavelengths as the temperature decreases to cryogenic values (Fig. 11 and 17). This is particularly observed for the grain sizes 20-50 μm (both samples) and 75-100 μm (hexahydrite). The band position for the 3-μm band was difficult to compute for the larger grain sizes because of the saturation of the band. In the case of epsomite, the higher number of water molecules causes the band saturation to occur also at intermediate grain size (75-100 μm). Although some authors report that the water band at 3 μm is insensitive to temperature variations (Jamieson et al., 2012), here we observe some correlation as mentioned above. On the other hand, when we look at all the other absorption features, we can see that band positions shift towards longer wavelengths. For hexahydrite, the 1.9-μm band position shows a systematic correlation with temperature, with the band center shifting towards longer wavelengths at cryogenic temperatures (hexahydrite, Fig. 9). For epsomite, the features at 1.5, 1.62 and 1.9 μm all show a correlation with T, again shifting towards longer wavelengths at cryogenic temperatures. We note that in water ice the corresponding absorption bands at 1.5, 1.65, and 1.99 μm also display strong spectral shifts in the same direction (Grundy and Schmitt 1998). The band area also shows different trends with decreasing temperature: it becomes larger for all absorption features in both materials, except the 3-μm band, for which a decrease at cryogenic temperatures is observed. The different behavior of the 3-μm band with respect to the other features described previously could be attributed to the fact that the H_2O-band tends to become deeper and narrower at low temperatures: the high wavelength edge shifts towards shorter wavelengths (Fig. 1 and 2).

Application to remote sensing

In order to interpret remote-sensed data and to discriminate among different types of hydrated sulfates, however, the 3-μm feature seems to be in any case poorly diagnostic, in particular due to its high degree of saturation linked to the high water content of these minerals. It is discernible in hexahydrite for the grain sizes 20-50 and 75-100 μm, while in epsomite it is only recognizable for the smallest grain size. Moreover, it is hard to retrieve a precise band center, due to band broadness or because it saturates and loses individuality. On the contrary, the features at 1.5 and 1.9 μm prove to be more diagnostic for mineral discrimination. At cryogenic temperatures, hexahydrite and epsomite can be fundamentally discriminated by looking at: (i) the fine structure of the 1.5-μm band, which is resolved into a triplet (hexahydrite) or into a doublet (epsomite) at spectral resolution of about 20 nm, and (ii) the 1.9-μm band, which has a defined V-shape at low temperatures (hexahydrite) or appears more flattened and composed by different minima (epsomite). The JUICE/MAJIS spectrometer (Piccioni et al., 2014; Langevin et al., 2014) with its high spectral sampling (3-7 nm in the 0.4-5.7-μm spectral range) will have great possibilities to discriminate among the different mineralogical phases on the surface of the icy Galilean satellites.

5. Conclusions

We have performed spectroscopic analyses on two poly-hydrated magnesium sulfates, hexahydrite and epsomite, in the visible and infrared range 0.5-4.0 μm; our measurements have been carried out at different temperatures, from room temperature (298 K) down to cryogenic values (minimum value being ~93 K). The obtained spectra of these samples and the subsequent derivation of band parameters has allowed us to investigate the fine structure of several absorption features arising at cryogenic temperatures. The spectra of hydrated sulfates are dominated by absorptions due to OH ions and H_2O molecules present in the mineral structure; trends of band parameters *vs*. temperature have been derived, showing a general narrowing and refining of bands, together with slight shifts of their positions.

Laboratory investigations of hydrated minerals, by means of visible and infrared spectroscopy, are key to support the interpretation of remote sensing data returned by ongoing interplanetary missions (e.g., NASA/Dawn) and future missions currently under implementation (e.g., ESA/ExoMars 2020, NASA/Europa Multiple Flyby Mission, ESA/JUICE). Detailed studies on the spectral behavior of hydrated minerals (silicates, sulfates) at cryogenic temperatures have implications in the correct interpretation of spectral data of Mars as well as of the icy Galilean satellites. Laboratory characterization is helpful in the possible identification and discrimination of this type of minerals, whose spectral features are considerably influenced by temperature variations, on surfaces of rocky planetary bodies; the presence of hydrated sulfates has important

implications on the understanding of the geologic processes that occurred on such Solar System bodies. The presence of mono- and poly-hydrated sulfates on other Solar System bodies would be strictly related to geologic processes that have occurred in presence of liquid water, such as evaporation from standing water-bodies (e.g. lakes), sedimentation, or weathering of primary minerals, with potential subsequent astrobiological implications.

Acknowledgements

The hydrated minerals and set of measurements described in this work are part of the research project: "Key laboratory measurements for Solar System ices" (PI: Dr. Federico Tosi), funded in 2013 by INAF-IAPS in the framework of an internal call for original research projects not otherwise funded. ASI funded and supported measurements campaign. Funding and support from the Centre National d'Etude Spatiale and the Programme National de Planétologie are acknowledged.

References

Beck P., Schmitt B., Cloutis E.A., Vernazza P.: *Low-temperature reflectance spectra of brucite and the primitive surface of 1-Ceres?*, Icarus 257, 471–476, 2015

Bibring J-P., A. Soufflot, M. Berthé, Y. Langevin, B. Gondet, P. Drossart, M. Bouyé, M. Combes, P. Puget, A. Semery, G. Bellucci, V. Formisano, V. Moroz, V. Kottsov and the OMEGA Co-I team, OMEGA: *Observatoire pour la Minéralogie, l'Eau, les Glaces et l'Activité*, in Mars Express: the scientific payload. Ed. by Andrew Wilson, scientific coordination: Agustin Chicarro, ESA Publications Division, ISBN 92-9092-556-6, p. 37 – 49, 2004

Bonnefoy N. *Développement d'un spectrophoto-goniomètre pour l'étude de la réflectance bidirectionnelle des surfaces géophysiques. Application au soufre et perspectives pour le satellite Io*. *PhD thesis,* Université Joseph Fourier, Grenoble, 2001

Brearley A.J. and Jones R.H.: *Chondritic Meteorites*, in: Papike, J.J. (Ed.), Planetary Materials. In: Reviews in Mineralogy, vol. 36. Mineralogical So- ciety of America, Washington, DC. Chap. 3

Brissaud O., Schmitt B., Bonnefoy N., Douté S., Rabou P., Grundy W., and Fily M.: *Spectrogonio radiometer for the study of the bidirectional reflectance and polarization functions of planetary surfaces. 1. Design and tests*, Applied Optics, Vol.43, Issue 9, pp. 1926-1937, http://dx.doi.org/10.1364/AO.43.001926, 2004

596 Brueckner J.: *Determination of chemical composition of soils and rocks at the MER landing sites*
597 *Gusev crater and Meridiani Planum using the APXS*, American Geophysical Union, Spring Meeting
598 2004, abstract #V11A05

599 Burgess R., Wright I.P., Pilliinger C.T.: *Determination of Sulphur-bearing components in C1 and C2*
600 *carbonaceous chondrites by stepped combustion*, Meteoritics, 26, 55-64, 1991

601 Carlson R.W., Calvin W.M., Dalton J.B., Hansen G.B., Hudson R.L., Johnson R.E., McCord T.B.,
602 Moore M.H.: *Europa's surface composition*, Europa, Edited by Robert T. Pappalardo, William B.
603 McKinnon, Krishan K. Khurana, University of Arizona Press, Tucson. The University of Arizona space
604 science series ISBN: 9780816528448, p.283, 2009

605 Chevrier V. and Mathè P.E.: *Mineralogy and evolution of the surface of Mars: A review*, Planetary
606 and Space Science, 55, 289-314, 2007

607 Chou I-M. and Seal II R.R.: *Magnesium and calcium sulfate stabilities and the water budget of*
608 *Mars*, Journal Of Geophysical Research, VOL. 112, E11004, doi:10.1029/2007JE002898, 2007

609 Clark R.N. and Roush T.L.: *Reflectance Spectroscopy: Quantitative Analysis Techniques for Remote*
610 *Sensing Applications*, Journal of Geophysical Research, VOL. 89, NO. B7, PAGES 6329-6340, 1984

611 Clark R.N., King T.V.V., Klejwa M., Swayze G.: *High spectral resolution reflectance spectroscopy of*
612 *minerals*, Journal of Geophysical Research, Vol.95, No.B8, pp.12653-12680, 1990

613 Clark, R. N., Chapter 1: Spectroscopy of Rocks and Minerals, and Principles of Spectroscopy, in
614 Manual of Remote Sensing, Volume 3, Remote Sensing for the Earth Sciences, (A.N. Rencz, ed.)
615 John Wiley and Sons, New York, p 3- 58, 1999

616 Cloutis E.A., Hawthorne F.C., Mertzman S.A., Krenn K., Craig M.A., Marcino D., Methot M., Strong
617 J., Mustard J.F., Blaney D.L., Bell III J.F., and Vilas F.: *Detection and discrimination of sulfate*
618 *minerals using reflectance spectroscopy*, Icarus 184, 121–157, 2006

619 Cloutis E.A., Craig M.A., Mustard J.F., Kruzelecky R.V., Jamroz W.R., Scott A., Bish D.L., Poulet F.,
620 Bibring J-P., and King P.L.: *Stability of hydrated minerals on Mars*, Geophysical Research Letters,
621 vol.34, L20202, doi:10.1029/2007GL031267, 2007

622 Craig M., Cloutis E.A., Kaletzke L., McCormack K., and Stewart L.: *Alteration Of Hydration*
623 *Absorption Features In Reflectance Spectra Of Selected Sulfates In A Low Pressure Environment:*
624 *0.45-4.3 μm*, Lunar and Planetary Science XXXVII, abstract n.2112, 2006

625 Crowley J.K.: *Visible and Near-Infrared (0.4-2.5 μm) Reflectance Spectra of Playa Evaporite*
626 *Minerals*, Journal Of Geophysical Research, VOL. 96, NO. B10, PAGES 16,231-16,240, 1991

627 Dalton III J.B., Prieto-Ballesteros O., Kargel J.S., Jamieson C.S., Jolivet J., Quinn R.: *Spectral*
628 *comparison of heavily hydrated salts with disrupted terrains on Europa*, Icarus 177, 472–490, 2005

629 Dalton III J.B.: *Linear mixture modeling of Europa's non-ice material based on cryogenic laboratory*
630 *spectroscopy*, Geophysical Research Letters, VOL. 34, L21205, doi:10.1029/2007GL031497, 2007

631 Dalton III J.B., Pitman K.M., Jamieson C.S., Dobrea N.: *Spectral properties of Hydrated Sulfate*
632 *Minerals on Mars*, EPSC Abstracts, Vol.6, EPSC-DPS2011-650, EPSC-DPS Joint Meeting, 2011

633 Dalton III J.B. and Pitman K.M.: *Low temperature optical constants of some hydrated sulfates*
634 *relevant to planetary surfaces*, Journal Of Geophysical Research, VOL. 117, E09001,
635 doi:10.1029/2011JE004036, 2012

636 Ehlmann B.L. and Edwards C.S.: *Mineralogy of the Martian Surface*, Annual Reviews Earth
637 Planetary Science, 42, 291-315, 2014

638 Feldman W.C., Mellon M.T., Maurice S., Prettyman T.H., Carey J.W., Vaniman D.T., Bish D.L., Fialips
639 C.I., Chipera S.J., Kargel J.S., Elphic R.C., Funsten H.O., Lawrence D.J., and Tokar R.L.: *Hydrated*
640 *States of MgSO4 at equatorial latitudes on Mars*, Geophysical Research Letters, vol.31, L16702,
641 doi:10.1029/2004GL020181, 2004

642 Fredriksson K. and Kerridge J.F.: *Carbonates and Sulfates in CI Chondrites: Formation by Aqueous*
643 *Activity on the Parent Body*, Meteoritics, 23, pp.35-44, 1988

644 Gendrin A., Mangold N., Bibring J-P., Langevin Y., Gondet B., Poulet F., Bonello G., Quantin C.,
645 Mustard J., Arvidson R., LeMouèlic S.: *Sulfates in Martian Layered Terrains: the OMEGA/Mars*
646 *Express View*, Science, Vol. 307, p.1587-1590, 2005

647 Gounelle, M. and Zolensky, M.E.: *A terrestrial origin for sulfates veins in CI1 chondrites*, Meteoritics
648 and Planetary Science, 36, 1321-1329, 2001

649 Grisolle F. *Les condensats saisonniers de Mars : étude expérimentale de la formation et du*
650 *métamorphisme de glaces de CO_2. PhD thesis,* Université Joseph Fourier, Grenoble, 2013

651 Grisolle F., Schmitt B., Beck P., Philippe S., and Brissaud O.: *Experimental simulation of the*
652 *condensation and metamorphism of seasonal CO_2 condensates under martian conditions*,
653 European Planetary Science Congress, EPSC Abstracts Vol. 9, EPSC2014-635-1, 2014

654 Hunt G.R.: *Spectral Signatures of Particulate Minerals in the Visible and Near Infrared*, Geophysics,
655 vol.42, n.3, pp.501-513, 1977

656 Hutchison R.: *Meteorites, a petrologic, chemical and isotopic Synthesis*, Cambridge University
657 Press, Cambridge, UK, ISBN 0 521 47010 2, 2006

658 Jamieson C.S., Dobrea N., Dalton III J.B., Pitman K.M., and Abbey W.J.: *Grain size and temperature*
659 *effects on the interpretation of remote sensing spectra*, Asteroids, Comets, Meteors, ACM
660 conference, abstract n.6384, 2012

Langevin Y., Piccioni G., Eng P., Filacchione G., Poulet F. and the MAJIS team: *THE MAJIS VIS-NIR IMAGING SPECTROMETER FOR THE JUICE MISSION*, 45th Lunar and Planetary Science Conference, LPSC abstract n.2493, 2014

McCord T.B., Hansen G.B., Fanale F.P., Carlson R.W., Matson D.L., Johnson T.V., Smythe W.D., Crowley J.K:, Martin P.D., Ocampo A., Hibbitts C.A., Granahan J.C., the NIMS Team: *Salts on Europa's Surface Detected by Galileo's Near Infrared Mapping Spectrometer*, SCIENCE, VOL. 280, 1242-1245, DOI: 10.1126/science.280.5367.1242, 1998

McCord T.B., Hansen G.B., Matson D.L., Johnson T.V., Crowley J.K., Fanale F.P., Carlson R.W., Smythe W.D., Martin P.D., Hibbitts C.A., Granahan J.C., and Ocampo A.: *Hydrated salt minerals on Europa's Surface from the Galileo near-infrared mapping spectrometer (NIMS) investigation*, Journal of Geophysical Research, vol.104, No. E5, 11,827-11,851, 1999

McCord, T.B., Hansen, G.B., Hibbitts, C.A., 2001. *Hydrated salt minerals on Ganymede's surface: Evidence of an ocean below*. Science 292, 1523-1525.

McCord T.B., Hansen G.B., Combe J-P., Hayne P.: *Hydrated minerals on Europa's surface: An improved look from the Galileo NIMS investigation*, Icarus, 209, 639-650, doi:10.1016/j.icarus.2010.05.026, 2010

Murchie S.L., and CRISM team: *Compact Reconnaissance Imaging Spectrometer for Mars (CRISM) on Mars Reconnaissance Orbiter (MRO)*, Journal Of Geophysical Research, VOL. 112, E05S03, doi:10.1029/2006JE002682, 2007

Murchie S.L., Mustard J.F., Ehlmann B.L., Milliken R.E., Bishop J.L., McKeown N.K., Noe Dobrea E.Z., Seelos F.P., Buczkowski D.L., Wiseman S.M., Arvidson R.E., Wray J.J., Swayze G., Clark R.N., Des Marais D.J., McEwen A.S. and Bibring J-P.: *A synthesis of Martian aqueous mineralogy after 1 Mars year of observations from the Mars Reconnaissance Orbiter*, Journal Of Geophysical Research, VOL. 114, E00D06, doi:10.1029/2009JE003342, 2009

Nachon, M., Mangold, N., Clegg, S., Schröder, S., Forni, O., S, Gasnault, O., Lasue, J., Le Mouélic, S., Lewin, E., Maurice, S., Newsom, H., Wiens, R., Fabre C., Dromart G., Leveillé, R., Bridges, J., Ehlmann, B., Grotzinger, J., Dyar, D. and the MSL team: *Sulfate calcium veins observed by the ChemCam instrument onboard Curiosity*, European Planetary Science Congress, EPSC Abstracts Vol. 8, EPSC2013-534, 2013

Nathues A., M. Hoffmann, M. Schaefer, L. Le Corre, V. Reddy, T. Platz, E. A. Cloutis, U. Christensen, T. Kneissl, J.-Y. Li, K. Mengel, N. Schmedemann, T. Schaefer, C. T. Russell, D. M. Applin, D. L. Buczkowski, M. R. M. Izawa, H. U. Keller, D. P. O'Brien, C. M. Pieters, C. A. Raymond, J. Ripken, P. M. Schenk, B. E. Schmidt, H. Sierks1, M. V. Sykes, G. S. Thangjam & J.-B. Vincent: *Sublimation in bright spots on (1) Ceres*, Nature Letter, vol.528, pp.237-240, doi:10.1038/nature15754, 2015

Rice M.S., J.F. Bell III, A. Godber, D. Wellington, A.A. Fraeman, J.R. Johnson, K.M. Kinch, M.C. Malin, J.P. Grotzinger, and the MSL Science Team: *Mastcam multispectral imaging results from the Mars*

Science Laboratory investigation in Yellowknife Bay, European Planetary Science Congress, EPSC Abstracts Vol. 8, EPSC2013-762, 2013

Piccioni G., Langevin Y., Filacchione G., Poulet F., Tosi F., Eng P., Dumesnil C., Zambelli M., Saggin B., Fonti S., Grassi D. and F. Altieri F.: *MAJIS, the Moons And Jupiter Imaging Spectrometer, designed for the future ESA/JUICE mission*, Geophysical Research Abstracts Vol. 16, EGU2014-10925-2, EGU General Assembly 2014

Roach L.H., Mustard J.F., Murchie S.L., Bibring J-P., Forget F., Lewis K.W., Aharonson O., Vincendon M., and Bishop J.L.: *Testing evidence of recent hydration state change in sulfates on Mars*, Journal Of Geophysical Research, VOL. 114, E00D02, doi:10.1029/2008JE003245, 2009

Vaniman D.T., Bish D.L., Chipera S.J., Fialips C.I., Carey J.W. and Feldman W.C.: *Magnesium sulphate salts and the history of water on Mars*, Nature, vol.431, 663-665, doi:10.1038/nature/02973, 2004

Van Keulen L.M., McCord T.B., Hansen G.B., Hibbitts C.A., and Crowley J.K.: *The Effect Of Grain Size On The Near-Infrared Reflectance Spectra Of Some Hydrated Salt Minerals*, Lunar and Planetary Science XXXI, abstract n.1539, 2000

Wang A., Freeman J.F., Jolliff B.L., and Arvidson R.E.: *Conversion Of Crystalline $MgSO_4.XH_2O$ To The Hydrated Amorphous Phase – A Raman, NIR, and XRD Study*, Lunar and Planetary Science XXXVII, abstract n.2168, 2006

Warren J.K.: *Evaporites: Sediments, Resources and Hydrocarbons*, Springer-Verlag, Berlin Heidelberg, 2006

Warren J.K.: *Evaporites through time: Tectonic, climatic and eustatic controls in marine and nonmarine deposits*, Earth-Science Reviews 98, 217–268, 2010

Weitz C.M., Noe Dobrea E., and Wray J.J.: *Mixtures of clays and sulfates within deposits in western Melas Chasma, Mars*, Icarus, 251, 291-314, 2015

Wray J.J., Milliken R., Swayze G.A., Ehlmann B.L., Dundas C.M., Baldridge A.M., Andrews-Hanna J.C., and Murchie S.L.: *Evaporites in Martian Paleolakes: Observations and Implications*, American Geophysical Union, Fall Meeting 2009, abstract #P41B06